NANO · MICRO small
www.small-journal.com

Cation/Anion Dual-Vacancy Pair Modulated Atomically-Thin Se_X-Co_3S_4 Nanosheets with Extremely High Water Oxidation Performance in Ultralow-Concentration Alkaline Solutions

Xiangyao Gu, Shuangshuang Li, Wenqian Shao, Xueqin Mu, Yuxin Yang, Yu Ge, Weitao Meng, Guangxiang Liu, Suli Liu,* and Shichun Mu**

The density functional theory calculation results reveal that the adjacent defect concentration and electronic spin state can effectively activate the Co^{III} sites in the atomically thin nanosheets, facilitating the thermodynamic transformation of *O to *OOH, thus offering ultrahigh charge transfer properties and efficiently stabilizing the phase. This undoubtedly evidences that, for metal sulfides, the atom-scale cation/anion vacancy pair and surface electronic spin state can play a great role in enhancing the oxygen evolution reaction. Inspired by the theoretical prediction, interconnected selenium (Se) wired ultrathin Co_3S_4 (Se_x-Co_3S_4) nanosheets with Co/S (Se) dual-vacancies ($Se_{1.0}$-Co_3S_4-$V_{S/Se}$-V_{Co}) pairs are constructed by a simple approach. As an efficient sulfur host material, in an ultralow-concentration KOH solution (0.1 M), $Se_{1.0}$-Co_3S_4-$V_{S/Se}$-V_{Co} presents outstanding durability up to 165 h and a low overpotential of 289.5 mV at 10 mA cm^{-2}, which outperform the commercial Co_3S_4 nanosheets (NSs) and RuO_2. Moreover, the turnover frequency of $Se_{1.0}$-Co_3S_4-$V_{S/Se}$-V_{Co} is 0.00965 s^{-1} at an overpotential of 0.39 V, which is 5.7 times that of Co_3S_4 NSs, and 5.8 times that of commercial RuO_2. The finding offers a rational design strategy to create the multi-defect structure in catalysts toward high-efficiency water electrolysis.

1. Introduction

In the past two decades, hydrogen energy obtained by electrocatalytic water splitting has been developed rapidly.[1] Nevertheless, the unfavorable thermodynamics of oxygen evolution reaction (OER) becomes the bottleneck for water splitting.[2] Recently, spinel transition compounds, such as metal sulfides, selenides, and phosphides have attracted increasing attention owing to their diversity, abundance, relatively low cost, and high intrinsic electrochemical activity for the electrocatalytic OER.[3–5] Furthermore, the research shows that both the specific defect site and ultrathin nanosheet feature play an important role in regulating the electronic structures and interface coordination of such spinel transition compounds, facilitating OH^- adsorption.[4,6] Accordingly, by means of defect engineering, the sulfur vacancy (V_S) and more low-valence Co (i.e., lower Co^{3+}/Co^{2+} ratio in Co_3S_4) have been introduced or formed in metal sulfides.[7–9] As reported, Co with higher oxidation states can promote OER in spinel sulfurs compounds, yet it is relatively inactive for Co sites with the lower oxidation states.[9] Thus, determining the effects of atom vacancies, surface electronic spin states, and coordination changes in the electrochemical properties remains elusive.

With this point in mind, to effectively promote the multistep OER process, the design of hybrid catalysts with different types of spinel structures (octahedral and tetrahedral sites) has been contributed.[10–12] Especially, the spinel Co_3S_4 with predominantly exposed trivalent Co ions and rich sulfur groups in surfaces are very promising in boosting the OER electrocatalytic performance.[11,13] More importantly, the introduction of ion vacancy pairs into atomically nanosheet lattices may provide positive effects on OER electrocatalysis.[14–16] Following this concept, by means of defect engineering, the sulfur vacancy (V_S) and more low-valence Co (i.e., lower Co^{3+}/Co^{2+} ratio in Co_3S_4) have been introduced or formed in metal sulfides. Meanwhile, cation doping was shown to be an effective way to enhance the performance of OER by reducing the binding energy of water molecules or the binding energy of intermediates to the active

X. Y. Gu, S. S. Liu, W. Q. Shao, Y. X. Yang, Y. Ge, W. T. Meng, G. X. Liu, S. L. Liu
Key Laboratory of Advanced Functional Materials of Nanjing
Nanjing Xiaozhuang University
Nanjing 211171, China
E-mail: liugx@njxzc.edu.cn; liusuli@njxzc.edu.cn
X. Y. Gu
Guangxi Key Laboratory of Low Carbon Energy Materials
Guangxi Normal University
Guilin 541004, China
X. Q. Mu, S. C. Mu
State Key Laboratory of Advanced Technology
for Materials Synthesis and Processing
Wuhan University of Technology
Wuhan 430070, China
E-mail: msc@whut.edu.cn
S. C. Mu
Foshan Xianhu Laboratory of the Advanced Energy Science
and Technology Guangdong Laboratory
Xianhu hydrogen Valley
Foshan 528200, China
The ORCID identification number(s) for the author(s) of this article can be found under https://doi.org/10.1002/smll.202108097.

DOI: 10.1002/smll.202108097

site.[17] However, Co with higher oxidation states can promote the OER in spinel sulfur compounds, yet it is relatively inactive for Co sites with the lower oxidation states. Thus, how to easily control the synergistic manipulation of exposed atom defect sites and the electronic configuration of spinel compounds in atomic-level nanosheets is still very challenging.

To fulfill the formulation, by density functional theory (DFT) calculations, we first predict the spin state of Co sites in Co_3S_4 by interlacing selenium (Se) threaded ultrathin (Se_x-Co_3S_4) nanosheets (NSs) at an atomic level. The site-specific catalytic activity for OER is evaluated based on the critical role of the Se doping, anion (S/Se) vacancies, and cation (Co) vacancies in Se_x-Co_3S_4 NSs, which effectively activate the spin-state of Co^{III} and then enhance the conductibility of catalysts. This demonstrates that the appropriate combination of multi-atomic defect structures is conducive to release the catalytic capacity of the catalyst for electrochemical reactions. Inspired by the calculation results, $Se_{1.0}$-Co_3S_4-$V_{S/Se}$-V_{Co} NSs are designed and constructed. During the mixed-phase reaction, structurally disordered active sites can be created and the synergistic effect between the different elements is enhanced because of Co^{3+} and abundant S exposure, which has a positive impact on the generation of ion vacancies.[16,17] As expected, $Se_{1.0}$-Co_3S_4-$V_{S/Se}$-V_{Co} NSs show an extremely low overpotential and high stability in ultralow KOH solutions, rivaling the performances of most reported non-noble-metal catalysts in ultralow-concentration media.

2. Results and Discussion

DFT calculations were applied to uncover the synergistic effect of Se doping, S (Se) and Co vacancies, and optimal electronic spin state of the surface Co^{3+}.[18,19] Four types of structural models were constructed in the theoretical calculation: pristine Co_3S_4 (100), Se_x-Co_3S_4 (100), Se_x-Co_3S_4 (100) with S (Se) vacancies (Se_x-Co_3S_4-$V_{S/Se}$), and Se_x-Co_3S_4 (100) with Co vacancies (Se_x-Co_3S_4-V_{Co}) (Figure S1, Supporting Information). The density of states (DOS) near the Fermi level, mainly originated from the 3d state, was investigated to probe the interaction between doped Se and Co_3S_4 NSs.[19] As shown in **Figure 1**a,b, the *d*-band center of Co 3d shifts to the higher energy from −2.166 eV of Co_3S_4 to −1.749 eV of Se_x-Co_3S_4-$V_{S/Se}$, and the orbital hybridization of Co 3d causes an obvious electron delocalization in Se_x-Co_3S_4. These would increase the overall electrical conductivity of catalysts, and offer better electrochemical performance.[20] Meanwhile, Se-doping induces the change in the Co spin states from High spin ($t_{2g}^4e_g^2$) to Low spin ($t_{2g}^6e_g^0$) (Figure 1c,d), and the consequent Low spin Co^{3+} would distort due to an atom defect effect, and form a slightly distorted prism, leading to Lower e_g occupancy of Co^{3+} with stronger Co-O bonds.[21] This hinders the deprotonation of Co-OOH, resulting in a significant enhancement of the OER performance.[22,23] As can be seen from Figure 1e, the catalytic activity of Co_3S_4 and Se_x-Co_3S_4-V_{Co} on Co sites is restricted by the formation of OH*. In comparison, the potential-limiting step of Se_x-Co_3S_4 and Se_x-Co_3S_4-$V_{S/Se}$ on Co sites is assigned to the formation of O_2. In addition, the needed energy potential-limiting step for Co_3S_4 is larger than that of Se_x-Co_3S_4-$V_{S/Se}$ and Se_x-Co_3S_4-V_{Co}, which implies that Se_x-Co_3S_4 with S/Se and Co vacancies pairs can operate at a lower overpotential for OER.

Furthermore, scaling relations exist between the corresponding Gibbs free energies (ΔG_{OOH*}, ΔG_{OH*}, ΔG_{O*}) and *d*-band centers over the above considered Co sites. Obviously, the formation of Se dopants and atom vacancies pairs leads to the *d* states nearer to the Fermi level, facilitating the OER activity (Figure 1f).[19] Meanwhile, an obvious volcano relationship can be obtained by plotting η_{OER} as a function of *d*-band center. By comparing the Co_3S_4 (100), Se_x-Co_3S_4 (100), Se_x-Co_3S_4 (100) with S (Se) vacancies (Se_x-Co_3S_4-$V_{S/Se}$), and Se_x-Co_3S_4 (100) with Co vacancies (Se_x-Co_3S_4-V_{Co}), we can see that Se doping, S (Se) vacancies, and Co vacancies individually decrease the overpotential (Figure 1f). Overall, doping Se atoms indeed lower the spin energy of all compounds and expands the active catalytic sites (Figure 1g).

Under the illuminating instructions of the DFT calculation results, by a simply approach, we prepared interconnected Se doped wired ultrathin Co_3S_4 (Se_x-Co_3S_4) NSs. **Figure 2**a shows the synthetic strategy of Se_x-Co_3S_4 NSs via a wet-impregnation method involving chemical adsorption and anion exchange. Thus, the atomically dispersed Co and S (Se) dual-vacancies pairs Se_x-Co_3S_4 (Se_x-Co_3S_4-$V_{S/Se}$-V_{Co}) electrocatalyst was established by incorporating Se atoms into the framework of ultrathin Co_3S_4 NSs to realize a metal-to-ligand interaction, providing robust redox active sites and fast carrier transport.[24,25] In detail, both high-magnification transmission electron microscopy (TEM) (Figure 2b and Figure S2, Supporting Information) and high-angle annular dark-field scanning TEM (HAADF-STEM) (Figure 2c and Figure S3, Supporting Information) images show that $Se_{1.0}$-Co_3S_4-$V_{S/Se}$-V_{Co} has an ultrathin nanosheet configuration. The high-resolution TEM (HRTEM) observation (Figure 2d and Figure S3, Supporting Information) further identifies the lattice fringes with interplanar spacing of 0.28 and 0.33 nm, which can be assigned to the (311) and (220) planes of Co_3S_4 (JCFDS# 42-1448), respectively.[26] The selected area electron diffraction (SAED) pattern also reveals the existence of the cubic Co_3S_4 phase (Figure 2d). In addition, the average thickness of $Se_{1.0}$-Co_3S_4-$V_{S/Se}$-V_{Co} measured by atomic force microscopy (AFM) (Figure 2e) is ≈ 2.5 nm, which corresponds to the ultrathin Co_3S_4 NSs,[27,28] providing more active sites for OER. Meanwhile, from HAADF-STEM images, it can be seen that $Se_{1.0}$-Co_3S_4-$V_{S/Se}$-V_{Co} consists of parallel zigzag lines, in which the bright dots correspond to Se or S atoms and the dark dots are the signals of Co.[29] More importantly, obvious S (Se) and Co atom vacancies pairs can be found in the surface of Se_x-Co_3S_4 NSs, as indicated by the yellow dotted lines in Figure 2f–h. In addition, the intensity profiles along the selected rectangular regions also suggest the missing of S (Se) and Co atoms, and the uniform dispersion of Se dopants in the surface of $Se_{1.0}$-Co_3S_4-$V_{S/Se}$-V_{Co}. ≈18.03 wt% Se loading can be ascertained for $Se_{1.0}$-Co_3S_4-$V_{S/Se}$-V_{Co} by inductively coupled plasma optical emission spectrometry (ICP-OES) test (Table S1, Supporting Information).

As shown in **Figure 3**a, from the X-ray diffraction (XRD) patterns, the obtained Se_x-Co_3S_4 NSs are well indexed to cubic Co_3S_4 phase (JCPDS 42-1448), consistent with the analysis results of TEM and HRTEM (Figures S4–S6, Supporting Information).[26] In addition, the typical characteristic peaks of Se_x-Co_3S_4-$V_{S/Se}$-V_{Co} NSs do not shift, indicating the

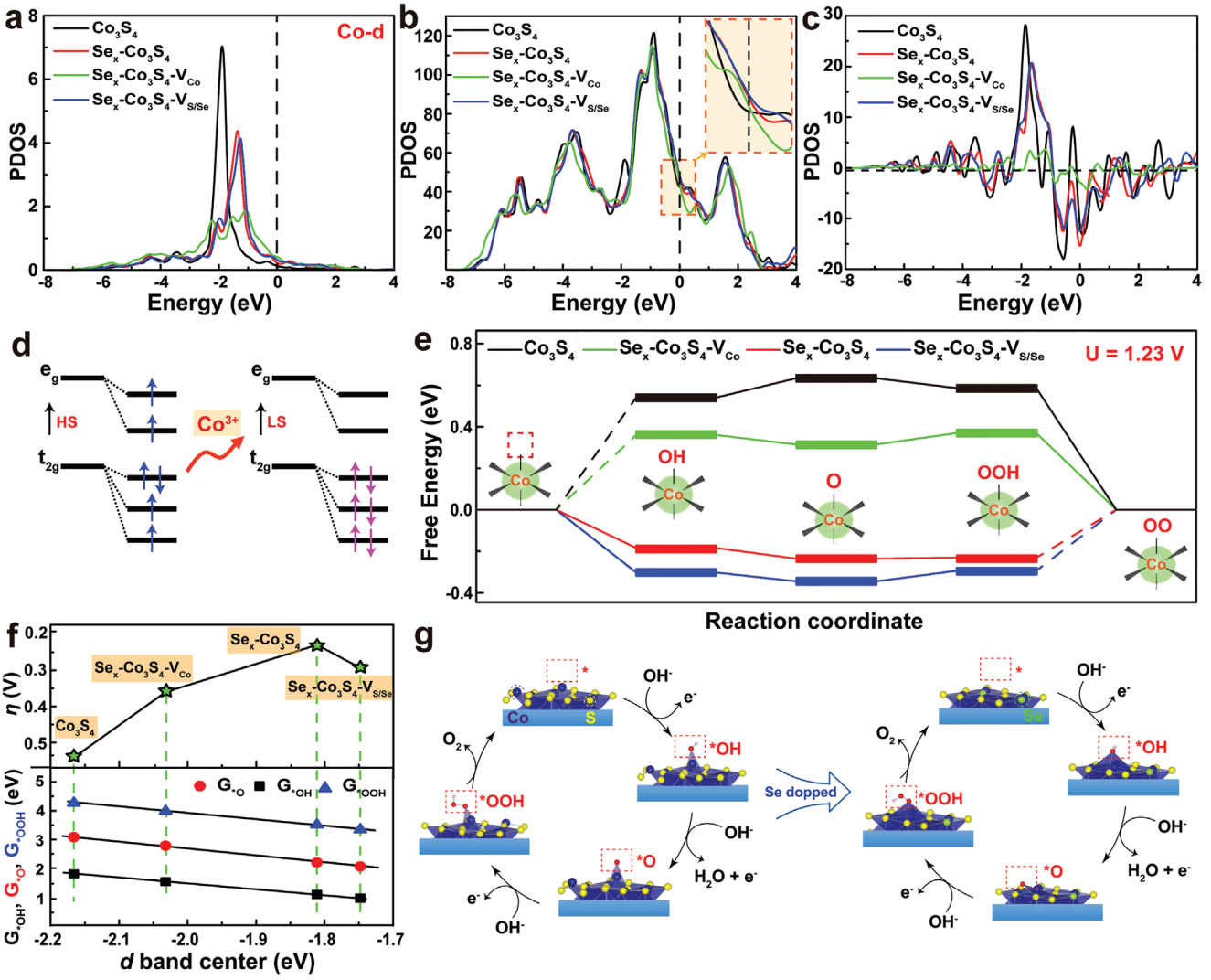

Figure 1. a–c) Calculated density of states for over the Co_3S_4 and Se_x-Co_3S_4. d) Schematic of the split of the 3d orbital of Co spin states. e) The energy profile for the OER process on the Co_3S_4 and Se_x-Co_3S_4. f) Scaling relation between ΔG_{OOH*}, ΔG_{OH*}, ΔG_{O*}, and *d*-band centers; volcano plot of overpotential as a function of *d*-band centers. g) Representative OER mechanism over the Co_3S_4 and Se_x-Co_3S_4.

unchanged interlayer stacking of Co_3S_4 NSs after intercalating Se, consistent with the observation result of HAADF-STEM in Figure 2f–h.[30] Additionally, the XPS survey spectra determine the presence of Co, Se, and S elements in samples (Figure S7 and Table S2, Supporting Information). In the Co 2p spectra (Figure 3b), there are two prominent peaks at the binding energies of 778.69 and 793.75 eV, and the second at 780.32 and 795.93 eV, respectively, which can be fitted with the two valence states of Co^{3+} and Co^{2+}.[15,26] From the S 2p spectrum of Se_x-Co_3S_4-$V_{S/Se}$-V_{Co} as shown in Figure 3c, two spin–orbit peaks for $Se_{1.0}$-Co_3S_4-$V_{S/Se}$-V_{Co} and S-O can be identified.[24] While for the Se 3d core level, its XPS spectrum (Figure 3d) can be deconvoluted into four main components, ascribed to the $3d_{5/2}$ and $3d_{3/2}$ of $Se_{1.0}$-Co_3S_4-$V_{S/Se}$-V_{Co}, respectively, and other two binding energies at 59.6 and 61.24 eV, corresponding to the surface oxidized species.[21] In particular, many characteristic peaks of surface oxidized species are observed, which signify possible surface oxidation of Se_x-Co_3S_4-$V_{S/Se}$-V_{Co} when exposed to the air. Notably, the binding energy of Co 2p or Se 3d for Se_x-Co_3S_4-$V_{S/Se}$-V_{Co} positively shifts compared to the initial Co_3S_4 catalyst, implying the decreased electron density of Co species due to the introduction of Se dopants and the formation of the atom S (Se) and Co vacancies pairs (Figure 3e). The electron paramagnetic resonance (EPR) spectrum further determines the amount of S and Co vacancies pairs. Compared with Co_3S_4, the lower intensity of the EPR signal can be found in Se_x-Co_3S_4-$V_{S/Se}$-V_{Co}, further indicating atom vacancies concentration can be optimized due to the Se doping effect (Figure 3f).[31] Moreover, the shift phenomenon for the spectral weight to higher magnetic fields in Figure 3f further infers the existence of intermediate spin in Se_x-Co_3S_4-$V_{S/Se}$-V_{Co}.

To understand how atomically dispersed cation/anion dual-vacancies pairs affect the OER catalytic performance, the prepared Se_x-Co_3S_4-$V_{S/Se}$-V_{Co} NSs and Co_3S_4 NSs as benchmark were subjected to systematic electrochemical evaluation by a three-electrode system in ultralow concentration alkaline solutions

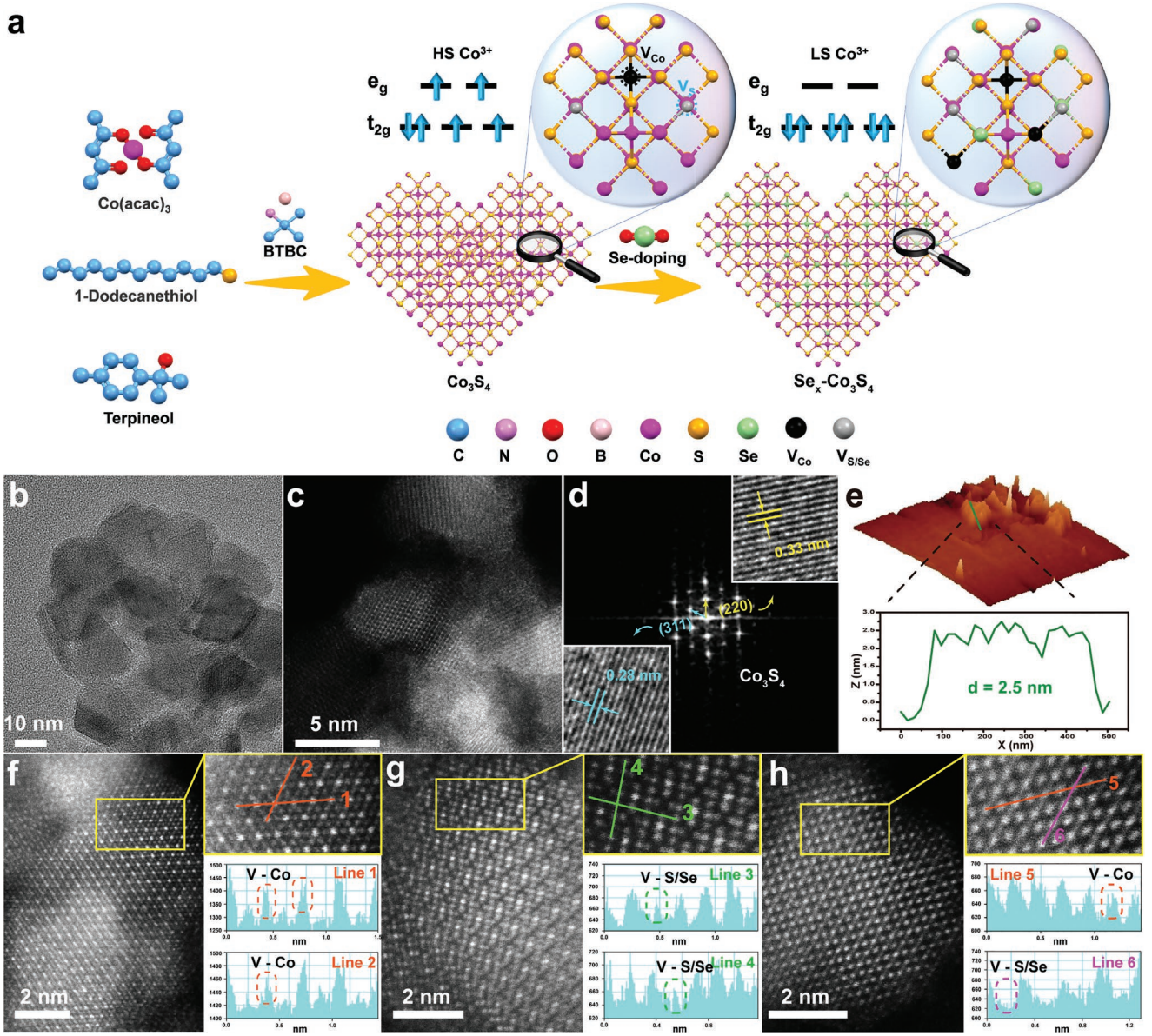

Figure 2. a) Synthetic strategy for Se_x-Co_3S_4 NSs. b) High-magnification TEM image, c) HAADF-STEM images of $Se_{1.0}$-Co_3S_4-$V_{S/Se}$-V_{Co}. d) HRTEM and SAED analysis of $Se_{1.0}$-Co_3S_4-$V_{S/Se}$-V_{Co}. e) AFM image of $Se_{1.0}$-Co_3S_4-$V_{S/Se}$-V_{Co} and the corresponding height profile. f–h) High-resolution HAADF-STEM images of different catalysts and the intensity profiles along the selected rectangular regions suggest the missed surface Se and Co atoms in $Se_{1.0}$-Co_3S_4-$V_{S/Se}$-V_{Co} NSs, respectively.

(0.1 M KOH).[32,33] **Figure 4**a shows the OER linear sweep voltammetry (LSV) curves of the samples. To deliver a current density of 10 mA cm^{-2}, $Se_{1.0}$-Co_3S_4-$V_{S/Se}$-V_{Co} exhibits the lowest overpotential (η) of 289.5 mV, in comparison with $Se_{1.5}$-Co_3S_4-$V_{S/Se}$-V_{Co} (313.8 mV), $Se_{0.5}$-Co_3S_4-$V_{S/Se}$-V_{Co} (309.7 mV), Co_3S_4 (323.5 mV), commercial RuO_2 and most Co-based OER catalysts (Table S3, Supporting Information). Obviously, the overpotential of $Se_{1.0}$-Co_3S_4-$V_{S/Se}$-V_{Co} is decreased by 34 mV compared with Co_3S_4 at a current density of 10 mA cm^{-2}, indicating the introduction of optimal atom vacancies does enhance the OER performance.

Furthermore, the kinetics of the OER was evaluated by calculating the Tafel slope of Se_x-Co_3S_4-$V_{S/Se}$-V_{Co} NSs and Co_3S_4 NSs. As shown in Figure 4b, $Se_{1.0}$-Co_3S_4-$V_{S/Se}$-V_{Co} possesses a Tafel slope of 67.5 mV dec^{-1}, smaller than that of $Se_{1.5}$-Co_3S_4-$V_{S/Se}$-V_{Co} (72.0 mV dec^{-1}), $Se_{0.5}$-Co_3S_4-$V_{S/Se}$-V_{Co} (74.4 mV dec^{-1}), Co_3S_4 NSs (80.63 mV dec^{-1}) and commercial RuO_2 (70.3 mV dec^{-1}), indicating the more rapid OER kinetics for $Se_{1.0}$-Co_3S_4-$V_{S/Se}$-V_{Co}.[34] Moreover, the turnover frequency (TOF) was calculated based on the Co center (Figure 4c). Of note, the TOF value of $Se_{1.0}$-Co_3S_4-$V_{S/Se}$-V_{Co} is 0.00965 s^{-1} at an overpotential of 0.39 V (Table S4, Supporting Information), which is 5.7 times that of Co_3S_4 NSs, and 5.8 times that of commercial RuO_2. The superior OER activity of $Se_{1.0}$-Co_3S_4 NSs can be ascribed to the synergistic effect of Se doping and Co/S (Se) vacancies pairs, consistent with our DFT-predicted results.

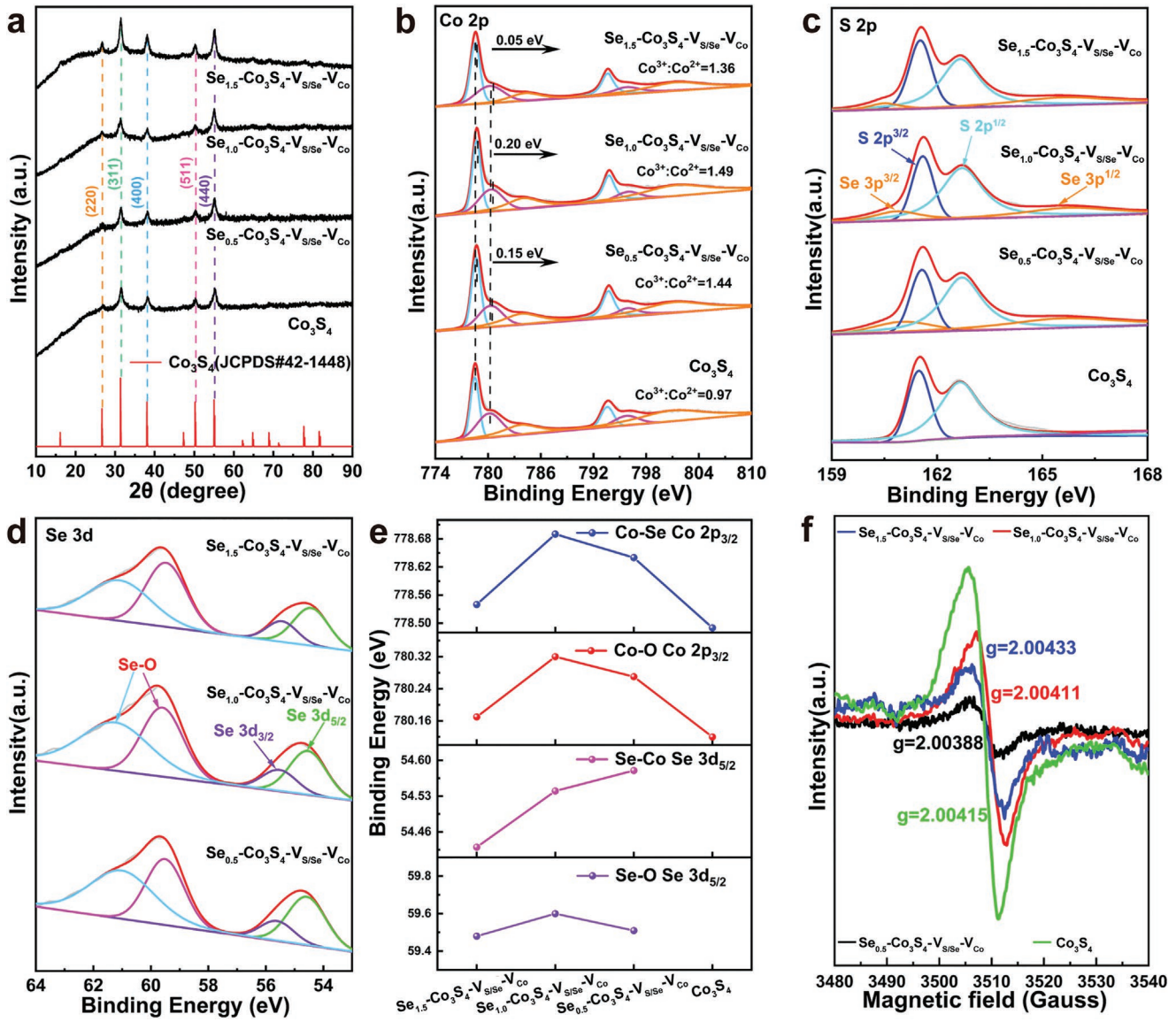

Figure 3. a) Powder XRD patterns of as-synthesized Se_x-Co_3S_4-$V_{S/Se}$-V_{Co} NSs. XPS spectra of the Se_x-Co_3S_4-$V_{S/Se}$-V_{Co} NSs and Co_3S_4 NSs: b) Co 2p, c) S 2p, and d) Se 3d. e) Binding energy shifts of Co-Se and Co-O peaks due to doping and vacancies. f) EPR spectra of the Se_x-Co_3S_4-V_S-V_{Co} NSs and Co_3S_4 NSs catalysts.

To further examine the catalytic process kinetics of Se_x-Co_3S_4- $V_{S/Se}$ -V_{Co} NSs, electrical impedance spectroscopy was performed. As shown in Figure 4d and Figure S8, Supporting Information, $Se_{1.0}$-Co_3S_4-$V_{S/Se}$-V_{Co} has a lower charge transfer resistance (R_{ct}) of 16.2 Ω compared with those of $Se_{0.5}$-Co_3S_4-$V_{S/Se}$-V_{Co} (29.1 Ω), $Se_{1.5}$-Co_3S_4-$V_{S/Se}$-V_{Co} (28.1 Ω), and Co_3S_4 NSs (36.0 Ω) at η = 289.5 mV, which corresponds to the highest charge transfer capability.[32] Furthermore, the electrochemical double-layer capacitance (C_{dl}) is followed by $Se_{1.0}$-Co_3S_4-$V_{S/Se}$-V_{Co} (136.2 mF cm^{-2}) > $Se_{0.5}$-Co_3S_4-$V_{S/Se}$ (75.4 mF cm^{-2}) > $Se_{1.5}$-Co_3S_4-V_{Co} (72.2 mF cm^{-2}) > Co_3S_4 (49.1 mF cm^{-2}), as shown in Figure 4e and Figure S9, Supporting Information, indicating the electrochemically active surface area (ECSA) of $Se_{1.0}$-Co_3S_4-$V_{S/Se}$-V_{Co} and other Se_x-Co_3S_4-$V_{S/Se}$-V_{Co} series samples.[34] These excellent properties allow Se_x-Co_3S_4-$V_{S/Se}$-V_{Co} NSs to possess higher OER activity than Co_3S_4 NSs. Moreover, it is also noteworthy that Se_x-Co_3S_4-$V_{S/Se}$-V_{Co} NSs outperform commercial IrO_2 and RuO_2 catalysts (Figure 4f and Table S3, Supporting Information), and previously reported spinel transition compounds evaluated via the RDE method.

More importantly, by means of chronoamperometry (j ≈ t) testing, $Se_{1.0}$-Co_3S_4-$V_{S/Se}$-V_{Co} NSs shows an outstanding long-term stability, with a negligible current decay over 165 h at a constant voltage operation (Figure 4g). The sample after stabilization test was further investigated by EPR and XPS measurements, proving the surface transformation of Se_x-Co_3S_4-$V_{S/Se}$-V_{Co} NSs into Se_x-Co_3S_4-OOH in the potential range (Figure 4h,i and Figure S10, Supporting Information), which are largely responsible for the boosted OER activity. As shown in Figure S11, Supporting Information, according to the TEM

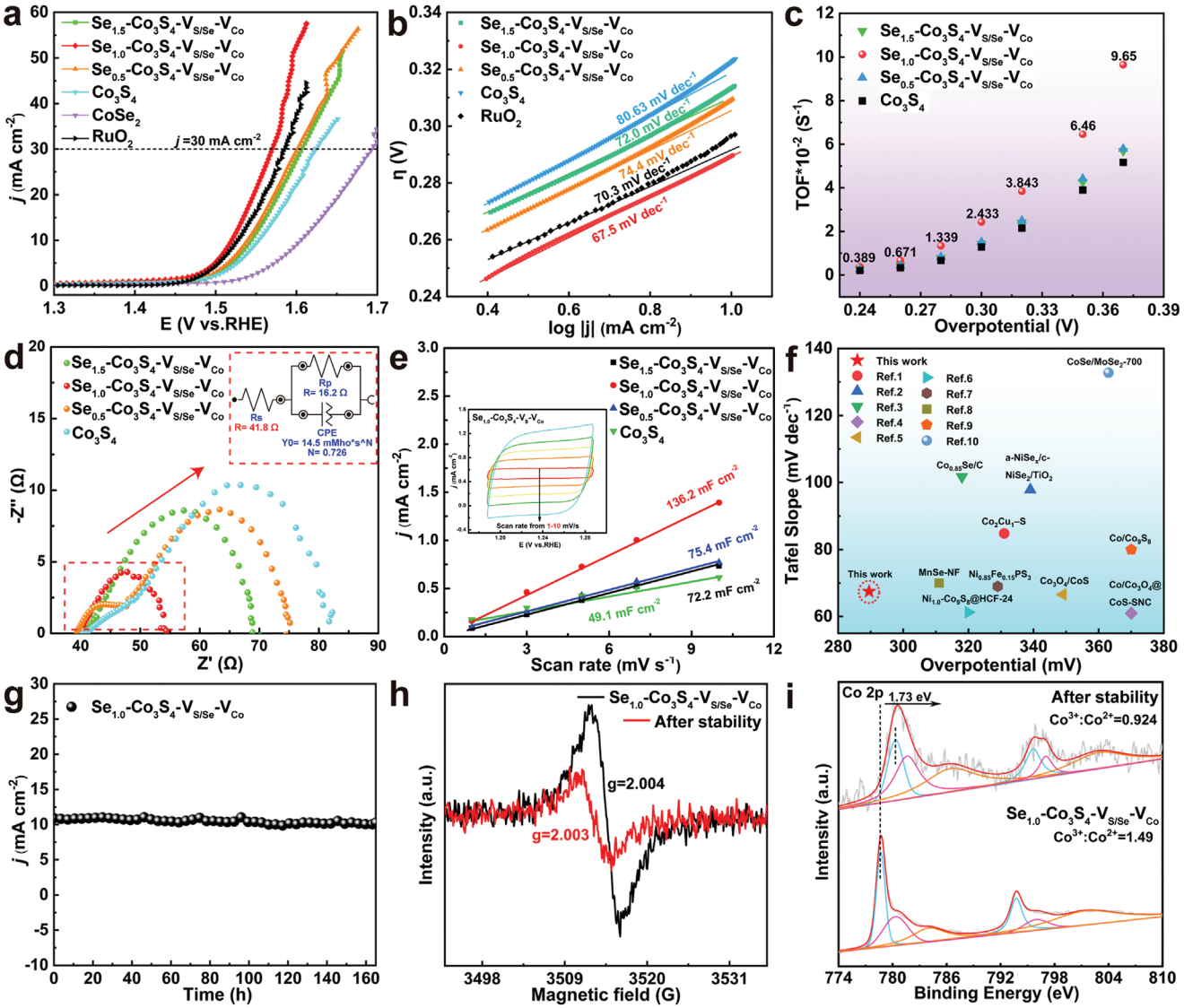

Figure 4. a) LSV curves of the Se_x-Co_3S_4-$V_{S/Se}$-V_{Co} NSs, $CoSe_2$, and RuO_2, respectively. b) Corresponding Tafel plots. c) TOF values calculated from the currents at different overpotentials. d) Nyquist plots of samples. e) Plots used for determination of the double-layer capacitance (C_{dl}) for Se_x-Co_3S_4-$V_{S/Se}$-V_{Co} NSs and Co_3S_4 NSs, respectively. f) The overpotential and Tafel slopes of some Co-based water oxidation electrocatalysts in alkaline electrolyte (Table S3, Supporting Information and the corresponding references). g) Chronoamperometry experiment response of $Se_{1.0}$-Co_3S_4-$V_{S/Se}$-V_{Co} NSs at 10 mA cm^{-2}. h) EPR of $Se_{1.0}$-Co_3S_4-$V_{S/Se}$-V_{Co} NSs after 165 h. i) XPS spectra of $Se_{1.0}$-Co_3S_4-$V_{S/Se}$-V_{Co} NSs after 165 h.

and STEM-EDS mapping images, there are no obvious morphology and structure changes for $Se_{1.0}$-Co_3S_4-$V_{S/Se}$-V_{Co} shows after stability test, confirming its excellent catalytic stability. All the results above demonstrate that the Se doped wired ultrathin Co_3S_4 nanosheets can not only effectively accelerate the charge transfer at atom vacancies and enhance the reaction kinetics but also optimize Low spin Co^{3+} to form active species, facilitating the electrochemical reaction.

3. Conclusion

In summary, to improve the OER performance of Co_3S_4, we launch Se doping and Co/S (Se) vacancies in Co_3S_4 nanosheets (NSs), as a rising star in electrocatalysts. Periodic DFT computations reveal that, with the existence of S (Se) and Co vacancies pairs, the energy barrier for Co atom diffusion is significantly decreased, implying the more favorable formation of the CoOOH phase. Experimentally, under ultralow-concentration KOH solution (0.1 M) conditions, the $Se_{1.0}$-Co_3S_4-$V_{S/Se}$-V_{Co} NSs display outstanding OER performance with an amazing long-term stability of at least 165 h and a low overpotential of 289.5 mV at a current density of 10 mA cm^{-2}. The prominent OER catalytic properties of Se_x-Co_3S_4-$V_{S/Se}$-V_{Co} NSs mainly caused by the following aspects: 1) the atom vacancies weaken the adsorption energy of the intermediate; 2) Se-dopants promote the formation of lower spin states of Co ions; 3) The Se doping can adjust the concentration of vacancies, and thus improve the stability of the catalyst. Undoubtedly, the proper combination of multiple atom defect structures is

promising to unlock the catalytic power of catalysts for various electrochemical reactions.

Supporting Information

Supporting Information is available from the Wiley Online Library or from the author.

Acknowledgements

This work was supported by the National Natural Science Foundation of China (NSFC) (21501096, 22075223), and Natural Science Foundation of Jiangsu (BK20150086, BK20201120), Foundation of the Jiangsu Education Committee (15KJB150020), the Six Talent Peaks Project in Jiangsu Province (JY-087), and Innovation Project of Jiangsu Province.

Conflict of Interest

The authors declare no conflict of interest.

Data Availability Statement

Research data are not shared.

Keywords

catalysts, dual-vacancies, phase stability, selenium doping, water oxidation

Received: December 30, 2021
Revised: January 21, 2022
Published online:

[1] H. Ding, H. F. Liu, W. S. Chu, C. Z. Wu, Y. Xie, *Chem. Rev.* **2021**, *121*, 13174.
[2] L. K. Gao, X. Cui, C. D. Sewell, J. Li, Z. Q. Lin, *Chem. Soc. Rev.* **2021**, *50*, 8428.
[3] P. X. Ji, X. Luo, D. Chen, H. H. Jin, Z. H. Pu, W. H. Zeng, J. W. He, H. W. Bai, Y. C. Liao, S. C. Mu, *ACS Sustainable Chem. Eng.* **2020**, *8*, 17851.
[4] Z. H. Xiao, Y.-C. Huang, C.-L. Dong, C. Xie, Z. J. Liu, S. Q. Du, W. Chen, D. F. Yan, L. Tao, Z. W. Shu, G. H. Zhang, H. G. Duan, Y. Y. Wang, Y. Q. Zou, R. Chen, S. Y. Wang, *J. Am. Chem. Soc.* **2020**, *142*, 12087.
[5] J. X. Feng, S. H. Ye, H. Xu, Y. X. Tong, G. R. Li, *Adv. Mater.* **2016**, *28*, 4698.
[6] J. Fu, F. M. Hassan, C. Zhong, J. Lu, H. Liu, A. P. Yu, Z. W. Chen, *Adv. Mater.* **2017**, *29*, 1702526.
[7] J. Q. Shan, C. Ye, S. M. Chen, T. L. Sun, Y. Jiao, L. M. Liu, C. Z. Zhu, L. Song, Y. Han, M. Jaroniec, Y. H. Zhu, Y. Zheng, S. Z. Qiao, *J. Am. Chem. Soc.* **2021**, *143*, 5201.
[8] Q. Zhao, Z. H. Yan, C. C. Chen, J. Chen, *Chem. Rev.* **2017**, *117*, 10121.
[9] M. Cabán-Acevedo, M. L. Stone, J. R. Schmidt, J. G. Thomas, Q. Ding, H.-C. Chang, M.-L. Tsai, J.-H. He, S. Jin, *Nat. Mater.* **2015**, *14*, 1245.
[10] M. L. Wu, M. J. Cui, L. P. Wu, S. Hwang, C. P. Yang, Q. Q. Xia, G. Zhong, H. Y. Qiao, W. T. Gan, X. Z. Wang, D. Kline, M. R. Zachariah, D. Su, T. Li, L. B. Hu, *Adv. Energy Mater.* **2020**, *10*, 2001119.
[11] X. F. Lu, S. L. Zhang, W. L. Sim, S. Y. Gao, X. W. (David) Lou, *Angew. Chem., Int. Ed.* **2021**, *60*, 22885.
[12] X. Y. Lu, H. R. Xue, H. Gong, M. J. Bai, D. M. Tang, R. Ma, T. Sasaki, *Nano-Micro Lett.* **2020**, *12*, 86.
[13] H. Y. Zeng, M. Oubla, X. P. Zhong, N. Alonso-Vante, F. Du, Y. Xie, Y. H. Huang, J. W. Ma, *Appl. Catal., B* **2021**, *281*, 119535.
[14] J. T. Li, D. Chu, H. Dong, D. R. Baker, R. Z. Jiang, *J. Am. Chem. Soc.* **2020**, *142*, 50.
[15] S. Liu, H. Cheng, K. Xu, H. Ding, J. Y. Zhou, B. J. Liu, W. S. Chu, C. Z. Wu, Y. Xie, *ACS Energy Lett.* **2019**, *4*, 423.
[16] a) Y. H. Dou, C. T. He, L. Zhang, H. J. Yin, M. Al-Mamun, J. M. Ma, H. J. Zhao, *Nat. Commun.* **2020**, *11*, 1664; b) Z. J. Liu, G. J. Wang, X. Y. Zhu, Y. Y. Wang, Y. Q. Zou, S. Q. Zang, S. Y. Wang, *Angew. Chem., Int. Ed.* **2020**, *59*, 4736.
[17] a) S. Niu, W. J. Jiang, Z. X. Wei, T. Tang, J. M. Ma, J. S. Hu, L. J. Wan, *J. Am. Chem. Soc.* **2019**, *141*, 7005; b) S. Zhang, S. E. Saji, Z. Y. Yin, H. B. Zhang, Y. P. Du, C. H. Yan, *Adv. Mater.* **2021**, *33*, 2005988; c) Q. C. Wang, X. X. Xue, Y. P. Lei, Y. C. Wang, Y. X. Feng, X. Xiong, D. S. Wang, Y. D. Li, *Small* **2020**, *16*, 2001571.
[18] Y. Z. Jin, Z. Li, J. Q. Wang, R. Li, Z. Q. Li, H. Liu, J. Mao, C. K. Dong, J. Yang, S. Z. Qiao, X. W. Du, *Adv. Energy Mater.* **2018**, *8*, 1703469.
[19] P. Z. Chen, Y. Tong, C. Z. Wu, Y. Xie, *Acc. Chem. Res.* **2018**, *51*, 2857.
[20] Z. P. Wang, Z. P. Lin, J. Deng, S. J. Shen, F. Q. Meng, J. T. Zhang, Q. H. Zhang, W. W. Zhong, L. Gu, *Adv. Energy Mater.* **2021**, *11*, 2003023.
[21] J. Suntivich, H. A. Gasteiger, N. Yabuuchi, H. Nakanishi, J. B. Goodenough, Y. S. -Horn, *Nat. Chem.* **2011**, *3*, 546.
[22] Z. Y. Zhang, Z. H. Zhu, *Appl. Surf. Sci.* **2021**, *570*, 151229.
[23] N. Xue, Z. Lin, P. Li, P. Diao, Q. Zhang, *ACS Appl. Mater. Interfaces* **2020**, *12*, 28288.
[24] J. Bai, J. Mei, T. Liao, Q. Sun, Z. G. Chen, Z. Q. Sun, *Adv. Energy Mater.* **2022**, *12*, 2103247.
[25] T. Liu, P. Li, N. Yao, T. Kong, G. Cheng, S. Chen, W. Luo, *Adv. Mater.* **2019**, *31*, 1806672.
[26] C. Zhang, Y. Shi, Y. Yu, Y. Du, B. Zhang, *ACS Catal.* **2018**, *8*, 8077.
[27] W. B. Wang, Y. Yang, Y. Zhao, S. Z. Wang, X. M. Ai, J. K. Fang, Y. W. Liu, *Nano Res.* **2022**, *15*, 872.
[28] W. W. Zhong, Z. P. Wang, N. Gao, L. G. Huang, Z. P. Lin, Y. P. Liu, F. Q. Meng, J. Deng, S. F. Jin, Q. H. Zhang, L. Gu, *Angew. Chem., Int. Ed.* **2020**, *59*, 22743.
[29] H. M. Sun, Z. H. Yan, F. M. Liu, W. C. Xu, F. Y. Cheng, J. Chen, *Adv. Mater.* **2020**, *32*, 1806326.
[30] F. Lu, Y. Zhang, S. Z. Liu, D. Y. Lu, D. Su, M. Z. Liu, Y. G. Zhang, P. Liu, J. X. Wang, R. R. Adzic, O. Gang, *J. Am. Chem. Soc.* **2017**, *139*, 7310.
[31] X. Z. Zhang, C. Q. Shang, E. M. Akinoglu, X. Wang, G. F. Zhou, *Adv. Sci.* **2020**, *7*, 2002037.
[32] S. L. Jiao, X. W. Fu, S. Y. Wang, Y. Zhao, *Energy Environ. Sci.* **2021**, *14*, 1722.
[33] Z. L. Zheng, L. Yu, M. Gao, X. Y. Chen, W. Zhou, C. Ma, L. H. Wu, J. F. Zhu, X. Y. Meng, J. T. Hu, Y. C. Tu, S. S. Wu, J. Mao, Z. Q. Tian, D. H. Deng, *Nat. Commun.* **2020**, *11*, 3315.
[34] Y. Huang, S. L. Zhang, X. F. Lu, Z. P. Wu, D. Luan, X. W. Lou, *Angew. Chem., Int. Ed.* **2021**, *60*, 11841.